ACS APPLIED MATERIALS & INTERFACES

Research Article

Cite This: ACS Appl. Mater. Interfaces 2018, 10, 11739−11746

www.acsami.org

High Br^- Content $CsPb(Cl_yBr_{1-y})_3$ Perovskite Nanocrystals with Strong Mn^{2+} Emission through Diverse Cation/Anion Exchange Engineering

Fei Li,[†] Zhiguo Xia,*[,†] Caofeng Pan,[‡] Yue Gong,[§] Lin Gu,[§] Quanlin Liu,[†] and Jin Z. Zhang[∥]

[†]The Beijing Municipal Key Laboratory of New Energy Materials and Technologies, School of Materials Sciences and Engineering, University of Science and Technology Beijing, Beijing 100083, P. R. China

[‡]Beijing Institute of Nanoenergy and Nanosystems, Chinese Academy of Sciences, CAS Center for Excellence in Nanoscience, National Center for Nanoscience and Technology (NCNST), Beijing 100083, P. R. China

[§]Beijing National Laboratory for Condensed Matter Physics, Institute of Physics, Chinese Academy of Sciences, Beijing 100190, P. R. China

[∥]Department of Chemistry and Biochemistry, University of California, Santa Cruz, California 95064, United States

Supporting Information

ABSTRACT: The unification of tunable band edge (BE) emission and strong Mn^{2+} doping luminescence in all-inorganic cesium lead halide perovskite nanocrystals (NCs) $CsPbX_3$ (X = Cl and Br) is of fundamental importance in fine tuning their optical properties. Herein, we demonstrate that benefiting from the differentiation of the cation/anion exchange rate, $ZnBr_2$ and preformed $CsPb_{1-x}Cl_3$:xMn^{2+} NCs can be used to obtain high Br^- content $Cs(Pb_{1-x-z}Zn_z)$-$(Cl_yBr_{1-y})_3$:xMn^{2+} perovskite NCs with strong Mn^{2+} emission, and the Mn^{2+} substitution ratio can reach about 22%. More specifically, the fast anion exchange could be realized by the soluble halide precursors, leading to anion exchange within a few seconds as observed from the strong BE emission evolution, whereas the cation exchange instead generally required at least a few hours; moreover, their exchange mechanism and dynamics process have been evaluated. The Mn^{2+} emission intensity could be further varied by controlling the replacement of Mn^{2+} by Zn^{2+} with prolonged ion exchange reaction time. White light emission of the doped perovskite NCs via this cation/anion synergistic exchange strategy has been realized, which was also successfully demonstrated in a prototype white light-emitting diode (LED) device based on a commercially available 365 nm LED chip.

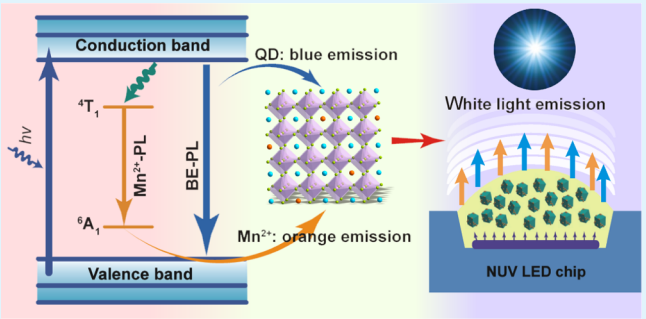

KEYWORDS: *perovskite nanocrystals, ion exchange, photoluminescence tuning, Mn^{2+} emission, white light LEDs*

INTRODUCTION

Colloidal all-inorganic cesium lead halide ($CsPbX_3$) perovskite nanocrystals (NCs) have attracted a great deal of attention in recent years because of their outstanding photoelectric properties[1−3] and facile chemical tunability of the band gap.[4−6] $CsPbX_3$ NCs are a promising alternative to II−VI and III−V semiconductor quantum dots (QDs) in various applications, such as low-threshold optically pumped lasers,[7,8] highly efficient light-emitting diodes (LEDs), detectors, and so on.[9,10] Many efforts have been also made to improve the stability and tune the optical properties of perovskite NCs.[11,12] Recently, perovskite NCs or QDs doped with transition-metal ions have been also explored with tunable properties.[13−16] The dopants in perovskite NCs not only achieve the objective of replacement of Pb^{2+} but also afford a way to introduce new optical, electronic, and magnetic properties.[4,17] Doping of perovskite NCs with Mn^{2+} has been studied because it potentially imparts both optical and charge carrier transport properties.[17,18] Mn^{2+}-doped perovskite NCs maintain the tetragonal crystalline structure of the $CsPbX_3$ host and exhibit strong band edge (BE) emission of Pb-based perovskite NCs. Additionally, Mn^{2+} substitution led to an additional characteristic emission of Mn^{2+} as well as enhancement of the photoluminescence quantum yields (PLQYs) of $CsPbCl_3$ from 5 to 54%.[19] As is well-known, the perovskite NCs suffer from thermal instability that severely restricted their practical applications. Such notorious thermal instability of $CsPbX_3$ NCs originates primarily from their low formation energies of perovskite lattices analogous to those of hybrid organic−inorganic halide perovskites. Interestingly, the formation energies of $CsPb_{1-x}X_3$:xMn perovskite NCs could be enhanced compared with those of their pure counterparts because of doping of Mn^{2+} in the host lattices and thereby fundamentally circumventing their poor thermal stability.[20]

Received: December 9, 2017
Accepted: March 16, 2018
Published: March 16, 2018

© 2018 American Chemical Society

DOI: 10.1021/acsami.7b18750
ACS Appl. Mater. Interfaces 2018, 10, 11739−11746

To date, compatible band alignment and efficient host exciton energy transfer to Mn^{2+} have not been achieved in Br^--dominant $CsPbX_3$ hosts. In previous studies, the poor emission intensity of Mn^{2+} in such hosts was ascribed to interplay among several competing processes for BE emission and Mn^{2+} emission, including BE electron−hole recombination and the Mn^{2+} $^4T_1-^6A_1$ transition, as well as forward and back energy transfer between the perovskite hosts and the Mn^{2+} ion.[21−23] The energy difference between the BE and Mn^{2+}-based transitions forcefully affected the competition between the latter two processes. With the increase of the Br^- content in the $CsPbX_3$ hosts, the energy difference become smaller, which reduced the forward energy transfer and strong Mn^{2+} emission, leading to reduced Mn^{2+} emission. However, the Mn^{2+} substitution ratio is extremely low in Br^--dominant $CsPbX_3$ hosts up to now, which impedes the study of the optical properties and energy-transfer mechanism in Br^--dominant $CsPb_{1-x}X_3$:$x$$Mn^{2+}$ NCs. Hence, heavy doping of Mn^{2+} in such NCs is highly desired to gain a deeper fundamental understanding of the above issues, and this requirement also becomes one of the motivations of this present work.

Here, we produced high Br^- content $CsPb_{1-x}(Cl_yBr_{1-y})_3$:$x$$Mn^{2+}$ perovskite NCs with strong Mn^{2+} emission via a diverse rate of ion exchange engineering (RIEE) strategy. The basic idea for RIEE originated from the different rates between anion exchange and cation exchange in lead halide perovskite NCs. The rate of anion exchange can be controlled by the solubility of the halide precursors, for which highly soluble precursors led to anion exchange within a few seconds, whereas the exchange with the less soluble salts was much slower.[24,25] To our best knowledge, the cation exchange in lead halide perovskite NCs generally required at least a few hours as indicated by the shift in the photoluminescence (PL) spectrum.[4] Motivated by the need to control the diverse ion exchange process, we employed the $ZnBr_2$ as precursors to react with preformed $CsPb_{1-x}Cl_3$:$x$$Mn^{2+}$ NCs to realize the doping of high-content Mn^{2+} in Br^--dominated perovskite NCs with strong Mn^{2+} emission. The RIEE reaction occurred between $ZnBr_2$ and preformed $CsPb_{1-x}Cl_3$:$x$$Mn^{2+}$ NCs as illustrated in Scheme 1. The red shift of BE emission from 392 to 474 nm occurred immediately, and the Mn^{2+} substitution ratio could stay at 22% in the $Cs(Pb_{1-x-z}Zn_z)(Cl_yBr_{1-y})_3$:$x$$Mn^{2+}$ NCs in a short ion exchange reaction time, which is not possible with the direct synthesis method or the halogen exchange method.[18,21] With the increase of the ion exchange reaction time, the intensity of Mn^{2+} emission was reduced because of the slow replacement of Mn^{2+} by Zn^{2+}. This phenomenon demonstrates that the Mn^{2+} content is another key factor that affects the intensity of Mn^{2+} emission in the high Br^- content $CsPb_{1-x}(Cl_yBr_{1-y})_3$:$x$$Mn^{2+}$ perovskite NCs. Moreover, the exchange of doped Mn^{2+} with Zn^{2+} can be controlled or even terminated by purification of the ion exchange system at different reaction times. Therefore, white light-emitting perovskite NCs have been prepared and used successfully in the fabrication of a prototype white LED device based on a commercially available 365 nm LED chip. This strategy opens up new opportunities to study the ion exchange process of doped halide perovskite NCs with diverse composition and the tunable PL, which will be also general for the preparation of other doped semiconductor QDs.

Scheme 1. Illustration of the Ion Exchange Process of Perovskite NCs with Different Ion-Exchange Reaction Rates between the Cation and Anion

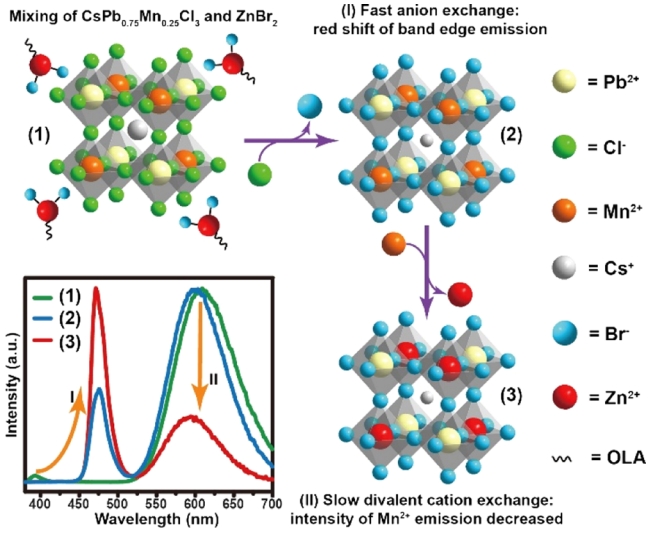

EXPERIMENTAL SECTION

Materials. Cs_2CO_3 (99.9%, Sinopharm), octadecene (ODE, 90%, Aladdin), oleic acid (OA, 90%, Aladdin), $PbCl_2$ (99.9%, Sinopharm), $ZnBr_2$ (99.9%, Aladdin), $MnCl_2$ (99%, Aladdin), oleylamine (OLA, Aladdin, 70%), hexane (99.9%, Sinopharm), and ethyl acetate (99%, Sinopharm) were used in this study. All chemicals were used as received.

Preparation of Cesium Oleate. Cesium oleate solution was prepared following the reported approach by Protesescu et al.[26] In brief, 1.2 mmol of Cs_2CO_3 and 1.2 mL of OA were loaded into a 3-neck flask along with 15 mL of ODE, degassed under vacuum at 120 °C for 0.5 h, followed by a second degassing phase at 150 °C under N_2 until clear solution was obtained.

Synthesis of $CsPb_xMn_{1-x}Cl_3$ NCs. ODE (10 mL), OLA (4 mL), OA (4 mL), $PbCl_2$ (0.36 mmol), and $MnCl_2$ (0.72−2.16 mmol) were loaded into a 50 mL 3-neck flask and dried under vacuum for 0.5 h at 120 °C. After complete solubilization of $PbCl_2$, the temperature was changed to 170 °C and a hot (~150 °C) Cs-oleate solution (1.2 mL, prepared as described above) was quickly injected, and the reaction mixture was immediately cooled by an ice-water bath.

Isolation and Purification of NCs. The NCs were extracted from the crude solution by centrifuging at 8000 rpm for 4 min. After centrifugation, the supernatant was discarded and the particles were redispersed in 10 mL of hexane. Then, the hexane solution was centrifuged for 4 min at 5000 rpm, and the precipitate was discarded. Subsequently, 20 mL of ethyl acetate was added to induce aggregation. The precipitate was collected by centrifuging at 9000 rpm for 4 min. Finally, 5 mL of hexane was added to the precipitate, resulting in a colloidal dispersion of $CsPb_xMn_{1-x}Cl_3$ NCs. We used ethyl acetate to induce aggregation, and typically, a large amount of antisolvent had to be added, with a ratio of 1:2, resulting in precipitation of the NCs.

Ion Exchange Reactions. Ion exchange precursor stock solutions were prepared by dissolving 0.30 mmol of $ZnBr_2$ in 10 mL of hexane, in the presence of 200 μL of OLA. The ion exchange reactions can be conducted under ambient conditions. A solution of $CsPb_xMn_{1-x}Cl_3$ QDs in hexanes was stirred at ambient temperatures, and the $ZnBr_2$ solution was added directly to the solution of former NCs. The amount of $ZnBr_2$ solution added was determined based on the desired band gap.

Fabrication of LEDs from $Cs(Pb_{1-x-z}Zn_z)(Cl_yBr_{1-y})_3$:$x$$Mn^{2+}$ NCs. In the preparation of the color conversion layer, $Cs(Pb_{1-x-z}Zn_z)(Cl_yBr_{1-y})_3$:$x$$Mn^{2+}$ NCs in hexane were mixed with the curable resin directly and then put in a vacuum chamber to remove the solvent.

DOI: 10.1021/acsami.7b18750
ACS Appl. Mater. Interfaces 2018, 10, 11739−11746

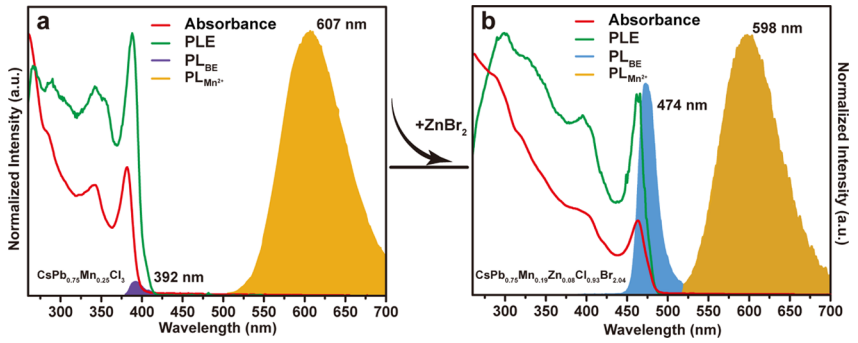

Figure 1. Spectral characterizations of Mn-doped perovskite NCs before and after the ion exchange reaction. (a) Electronic absorption and PL spectra of $CsPb_{0.75}Cl_3$:0.25Mn^{2+} NCs. $CsPb_{0.75}Cl_3$:0.25Mn^{2+} NCs exhibit dual-color emission, with the broad band peaked at ∼607 nm, arising from a Mn^{2+} d−d transition and the narrow band peaked at ∼392 nm attributed to BE emission. (b) Absorption and PL spectra of $CsPb_{0.75}Zn_{0.08}Cl_{0.93}Br_{2.04}$:0.19$Mn^{2+}$ after the ion exchange reaction for 4 h, and the BE emission is shifted to 474 nm because the Br^- incorporates into the host. Meanwhile, a strong Mn^{2+} emission was observed. The PLE spectrum for the Mn^{2+} emission is also red-shifted and resembles the absorption spectrum, indicating that Mn^{2+} is sensitized by the host NCs.

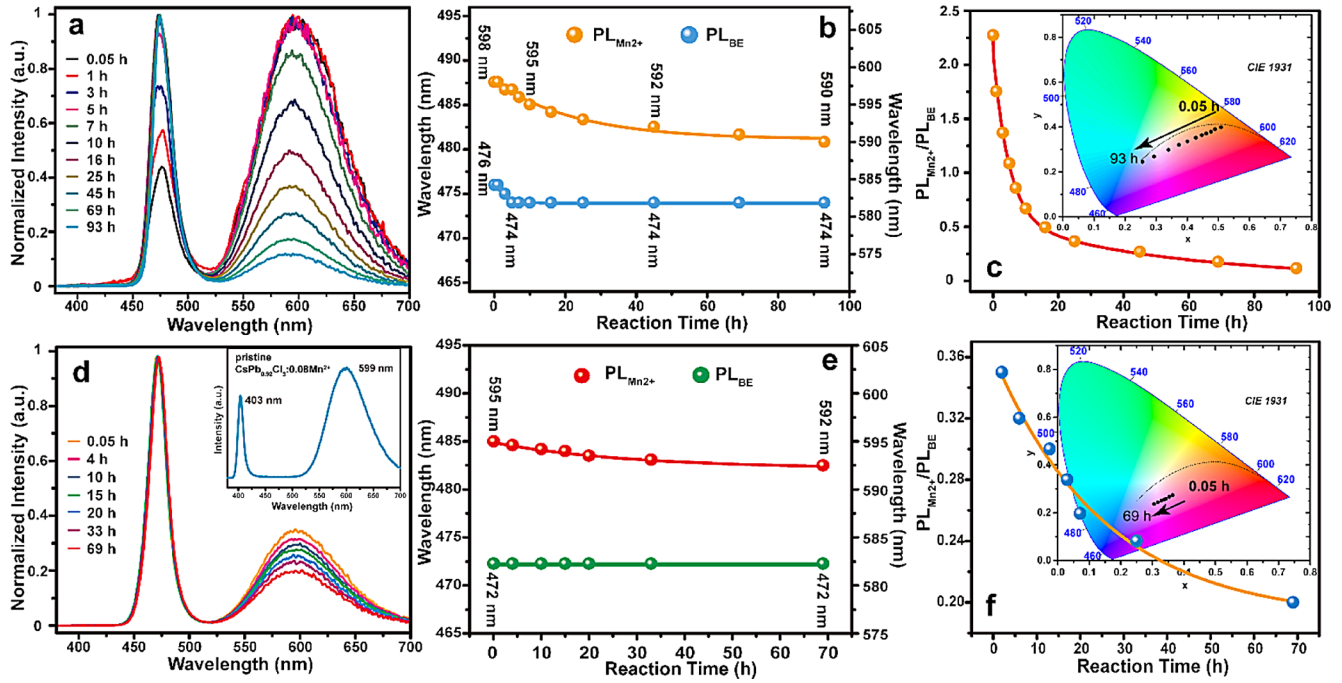

Figure 2. Spectral evolution of Mn^{2+}-doped $CsPb_{1-x}Cl_3$:xMn^{2+} NCs during the ion exchange reaction. (a,d) PL spectra of ion exchanged NCs collected at different reaction times using $CsPb_{0.75}Cl_3$:0.25Mn^{2+} and $CsPb_{0.92}Cl_3$:0.08Mn^{2+} as parent NCs, respectively. The inset of (d) is the PL spectra of $CsPb_{0.92}Cl_3$:0.08Mn^{2+} NCs. (b,e) Variation of peak positions of BE emission and Mn^{2+} emission. The peak of BE emission nearly locked at a certain wavelength at the very start of the ion exchange reaction. The peak of Mn^{2+} emission shifted to shorter wavelength with the increasing ion exchange time. (c,f) Intensity ratio of Mn^{2+} emission and BE emission collected at different ion exchange reaction times, and the color change has been also given in the CIE diagram in the corresponding insets.

Finally, the mixtures were coated onto commercial GaN LED chips with 365 nm emission operated at 5.0 V.

Characterization. X-ray diffraction (XRD) was performed on a PANalytical X'Pert^3 powder diffractometer equipped with a Cu Kα radiation source and operated at 40 kV and 40 mA. Transmission electron microscopy (TEM) was performed on a Tecnai F20 microscope operated at 200 keV on 200 mesh carbon-coated nickel grids. The UV−vis−NIR absorption spectra of colloidal solutions were collected at room temperature using a Varian Cary 5 spectrophotometer. The PL spectra were measured using a fluorescence spectrophotometer (FLSP920 fluorescence spectrophotometer, Edinburgh Instruments Ltd, UK). The luminescence decay curves were obtained using the same FLSP920 fluorescence spectrophotometer. The PLQY was measured by an absolute PLQY measurement system (C9920-02, Hamamatsu Photonics) with an integrating sphere at room temperature.

RESULTS AND DISCUSSION

The Mn^{2+}-doped $CsPbCl_3$ NCs exhibit electronic absorption and PL features that are very similar to those in previous reports[19] (Figure 1a). The PL emission spectrum shows dual emission peaks, including narrow BE emission peaked at 392 nm with full-width at half-maximum (fwhm) of ca. 110 meV and a broad PL band (fwhm ca. 260 meV) attributable to Mn^{2+} d−d emission, $^4T_1$−$^6A_1$ transition, peaked at ∼607 nm, independent of the dopant concentration.[27,28] The intensity of Mn^{2+} emission is ∼10 times stronger than that of the BE emission because the Mn^{2+} substitution reached 25% [as

DOI: 10.1021/acsami.7b18750
ACS Appl. Mater. Interfaces 2018, 10, 11739−11746

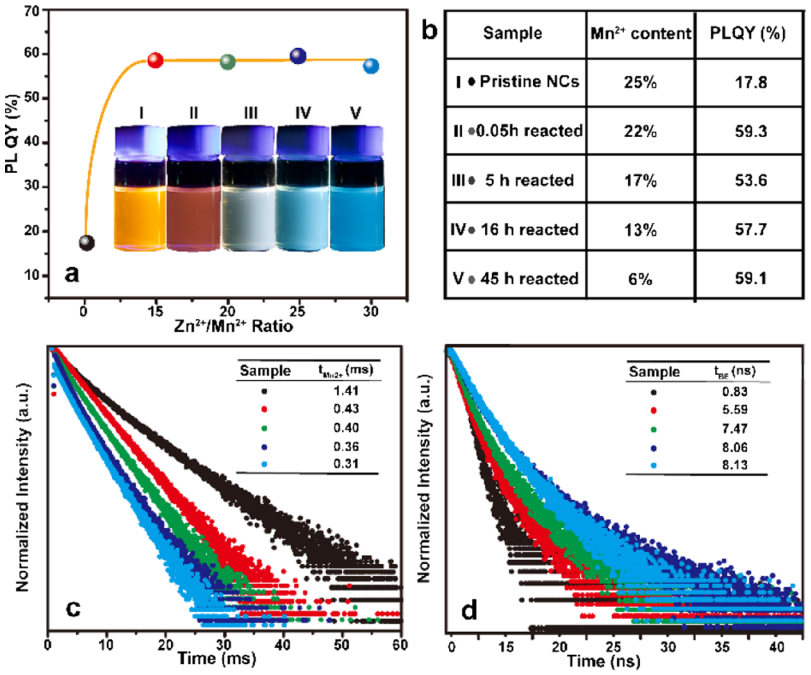

Figure 3. (a,b) PLQY and Mn^{2+} content of the initial and ion exchanged $CsPb_{0.75}Cl_3$:0.25Mn^{2+} NCs. The initial NCs have a low QY of 17.8%. After ion exchange, the QY of the samples sharply increases to 59.3% and maintains that level with the increasing ion exchange reaction time. The photographs of the pristine $CsPb_{0.75}Cl_3$:0.25Mn^{2+} NCs and ion exchanged NCs with different reaction times under 365 nm UV lamp illumination. The color changes come from the decrease of the Mn^{2+} content. (c,d) Time-resolved PL for the initial and ion exchanged $CsPb_{0.75}Cl_3$:0.25Mn^{2+} NCs.

determined by inductively coupled plasma atomic emission spectroscopy (ICP−AES)]. As the ion exchange was performed between $ZnBr_2$ and the as-synthesized $CsPb_{0.75}Cl_3$:0.25Mn^{2+} NCs with the reaction time of 4 h, the Mn^{2+} emission remains unchanged in the peak position throughout the exchange, whereas the BE emission peak shifts to 474 nm (Figure 1b). The chemical composition of such exchanged NCs with an exchange time of 4 h was measured to be $CsPb_{0.75}Zn_{0.08}Cl_{0.93}Br_{2.04}$:0.19$Mn^{2+}$.

In a previous study, the intensity ratio of Mn^{2+} emission and BE emission decreased with the increasing bromide content and the Mn^{2+} emission almost vanished when the host reached the expected halogen composition of perovskite NCs.[21] However, after the ion exchange occurred between $ZnBr_2$ and $CsPb_{0.75}Cl_3$:0.25Mn^{2+} NCs, strong Mn^{2+} emission, more intense than that of BE emission, could still be observed, although the change in the intensity ratio between the Mn^{2+} emission and BE emission decreased as well. The Mn^{2+}-doped and high Br^- content perovskite NCs with strong Mn^{2+} emission possess novel optical properties involving new pathways for energy transfer, as discussed later. Additionally, the PL excitation (PLE) spectrum collected by monitoring the PL of Mn^{2+} emission at 598 nm closely follows the absorption spectrum. This indicates that similar to Mn^{2+}-doped II−VI semiconductor NCs, the nominally forbidden Mn^{2+} emission is sensitized by the $CsPbX_3$ NCs host, confirming successful Mn^{2+} doping.[29,30]

The PL spectral evolution over time of Mn^{2+}-doped $CsPb_{0.75}Cl_3$:0.25Mn^{2+} NCs during ion exchange is given in Figure 2a. The intensity of the Mn^{2+} emission is stronger than that of BE emission at the very start (0.05 h) of the ion exchange reaction. With the increasing reaction time, the intensity of BE emission was enhanced and the intensity of Mn^{2+} emission decreased relatively. At the reaction time of 5 h, the intensity of the two emission bands became nearly the same, and with further increase in time, the intensity of the BE emission surpassed that of the Mn^{2+} emission. Notably, the peak positions of the BE emission were related with a different halide composition of the perovskite NCs, whereas the Mn^{2+} emission around 590 nm was dependent on the Mn^{2+} doped content. As can be seen in Figures 1a and 2b, the BE emission peak shifted from 392 nm for $CsPb_{0.75}Cl_3$:0.25Mn^{2+} to 474 nm for $CsPb_{0.73}Zn_{0.03}Cl_{0.91}Br_{2.05}$:0.22$Mn^{2+}$ at 0.05 h, with no significant change with the prolonging of reaction time. This phenomenon indicates that the halide exchange that occurred between $ZnBr_2$ and $CsPb_{0.75}Mn_{0.25}Cl_3$ NCs was very fast, which resulted in the constant halide composition during the ion exchange reaction. For the Mn^{2+} emission, the PL peak shifted monotonically to the blue, eventually reaching 590 nm, which can be attributed to the reduced Mn^{2+} content, causing the weakening of Mn−Mn interactions.[31,32] The time-dependent peak evolution of the Mn^{2+} emission indicates a much slower divalent cation exchange rate. The content of Mn^{2+} variation is also confirmed by ICP−AES that showed the halide composition being constant at the very start of the ion exchange reaction and the Mn^{2+} being replaced by Zn^{2+} slowly with the increase of the ion exchange reaction time, as shown in the Figure 3b.

To further understand the effect of the Mn^{2+} content on the intensity of Mn^{2+} emission in high Br^- concentration perovskite NCs, a similar ion exchange reaction was conducted by employing a small amount of Mn^{2+}-doped $CsPbCl_3$ NCs (8% Mn^{2+} substitution) as the parent NCs. The BE and Mn^{2+} emission peaks of $CsPb_{0.92}Cl_3$:0.08Mn^{2+} NCs are consistent with those of a previous study (inset of Figure 2d).[19] Additionally, the intensity of Mn^{2+} emission in the parent $CsPb_{0.92}Cl_3$:0.08Mn^{2+} NCs is just 1.24 times greater than that of BE emission, which is much smaller than that of the

DOI: 10.1021/acsami.7b18750
ACS Appl. Mater. Interfaces 2018, 10, 11739−11746

$CsPb_{0.75}Cl_3$:0.25Mn^{2+} NCs caused by the smaller amount of Mn^{2+} substitution. As the ion exchange reaction occurred, the PL spectral variation behavior was similar to that discussed above. However, the intensity of BE emission was stronger than that of the Mn^{2+} emission from the beginning of the ion exchange reaction, which is different from the above (Figure 2d). These results demonstrate that the intensity of the Mn^{2+} emission in high Br^- content $CsPb_{1-x}(Cl_yBr_{1-y})_3$:x$Mn^{2+}$ NCs is also related to the Mn^{2+} substitution ratio. Furthermore, as can be seen in Figure 2e, the PL peak shift behavior of BE and Mn^{2+} emission is similar to that of as-used $CsPb_{0.75}Cl_3$:0.25Mn^{2+} as parent NCs; however, the variation of the peak wavelength is minor. The color of the NCs changed with the prolonging reaction time as shown in Figure 3a, which is due to a change in the intensity ratio between Mn^{2+} and BE emission. Figure 2c shows the intensity ratio of Mn^{2+} and BE emission collected along with the reaction time. At the first 10 h of the ion exchange reaction, the intensity ratio of Mn^{2+} and BE emission decreased sharply. With the increasing reaction time, the change of this ratio became slower. The change of the intensity ratio between Mn^{2+} and BE emissions for the reaction that employed $CsPb_{0.92}Mn_{0.08}Cl_3$ NCs as parent NCs was slow at the beginning of reaction (Figure 2f). These results indicate the Mn^{2+} content is the key factor in controlling the rate of divalent cation exchange. Additionally, the Mn^{2+} content in the parent NCs could also influence the variation range of the CIE chromaticity coordinate, as shown in the inset of Figure 2c,f.

The measured PLQY for the selected samples is shown in Figure 3a. The pristine $CsPb_{0.75}Cl_3$:0.25Mn^{2+} NCs exhibit relatively low PLQY (<17.8%). Notably, after the ion exchange reaction, the PLQY increased to 59.3% (0.05 h product, with the chemical composition of $CsPb_{0.73}Zn_{0.03}Cl_{0.91}Br_{2.05}$:0.22$Mn^{2+}$). This trend is also in accordance with the result as reported by Klimov et al.[21] When such an ion exchange process performed continuously, the PLQY settled to a value ~56%, with a decrease of the Mn^{2+}/Zn^{2+} ratio. This is in contrast to a previous study that found that the loss of Mn^{2+} during the anion exchange reaction resulted in a decline of the PLQY of the Mn^{2+} emission in perovskite NCs.[21] To understand the difference, the PL lifetimes of Mn^{2+} and BE emission of the pristine $CsPb_{0.75}Cl_3$:0.25Mn^{2+} NCs and the product perovskite NCs were measured, as shown in Figure 3c,d. The Mn^{2+} emission in pristine and product NCs showed a single exponential decay, which can be fit with a lifetime value of 1.41 ms for the pristine $CsPb_{0.75}Cl_3$:0.25Mn^{2+} NCs. Upon ion exchange, the lifetime decreased first to 0.43 ms and finally to 0.31 ms. The relationship between PLQY (η) and the observed PL lifetime is given by the following general expression[33]

$$\eta = \frac{1/\tau_0}{1/\tau_1} \quad (1)$$

where τ_0 is the radiative lifetime and τ_1 is the observed PL lifetime ($\tau_1 = \tau_{avg}$ in this case). According to this relationship, the shorter the observed PL lifetime, the lower the PLQY is. Therefore, the PLQY of Mn^{2+} emission decreased with the replacement of Mn^{2+} by Zn^{2+} during this ion exchange reaction. However, the changes in the PL lifetime and PLQY of BE emission are different from that of the Mn^{2+} emission. BE emission showed two decay components for pristine and product NCs. The average lifetime can be determined using $\tau_{avg} = \sum A_i\tau_i^2/\sum A_i\tau_i$, where A_i and τ_i are amplitude and lifetime of individual components fit with exponentials, respectively. For the pristine $CsPb_{0.75}Cl_3$:0.25Mn^{2+} NCs reacted with $ZnBr_2$, the τ_{avg} increased from 0.83 ns for the pristine $CsPb_{0.75}Cl_3$:0.25Mn^{2+} NCs to 5.59 ns for the as-prepared NC product at 0.05 h. This result is mainly due to the replacement of Cl^- by Br^-. With the increased reaction time, the τ_{avg} further increased to 8.13 ns, which can be attributed to the decrease of the Mn^{2+} content. The PLQY also increased with the increasing PL lifetime in the $CsPbX_3$ (X = Cl, Br) perovskite system, as reported in previous works.[34] At the beginning of the reaction, there is more energy transferred from the perovskite host to the Mn^{2+} ion, leading to a relatively high PLQY for Mn^{2+} emission. With the increase of the reaction time, the BE electron−hole recombine preferentially because of the decrease in Mn^{2+} substitution by Zn^{2+}.[21] Thus, the PLQY of BE emission increased, whereas that of Mn^{2+} emission decreased, resulting in the settled value of PLQY during the ion exchange reaction.

The pristine NCs and as-obtained NCs after the ion exchange reaction exhibited a similar cubic morphology, as shown in Figure 4a−c. Both high-resolution TEM (inset of Figure 4a−c) and powder XRD (Figure 4d) show that the NCs are highly crystalline. Ion exchange did not change the cubic shape of the pristine $CsPb_{0.75}Cl_3$:0.25Mn^{2+} NCs (Figure 4a), although after exchanging with $ZnBr_2$ their size increased first, from 10 ± 1 to 12.2 ± 1.4 nm (Figure 4b), whereas continuous exchange reaction led to a slight decrease in size, to 11.8 ± 1.3 nm (Figure 4c). This size variation comes from the substitution of Cl^- (99 pm) with larger Br^- (114 pm) at the very start of the reaction and Mn^{2+} ions (97 pm) with smaller Zn^{2+} ions (74 pm) with a continuous exchange reaction. We also investigated the morphology evolution of the samples with $CsPb_{0.92}Cl_3$:0.08Mn^{2+} as pristine NCs, as shown in Figures S1 and S2. The trend of morphology evolution is similar to that of the heavily doped NCs, demonstrating the reproducibility of this ion exchange method. The XRD pattern collected on the pristine $CsPb_{0.75}Cl_3$:0.25Mn^{2+} NCs (Figure 4d) could be indexed as cubic $CsPbCl_3$ (a = 5.065 Å, space group $Pm\bar{3}m$,

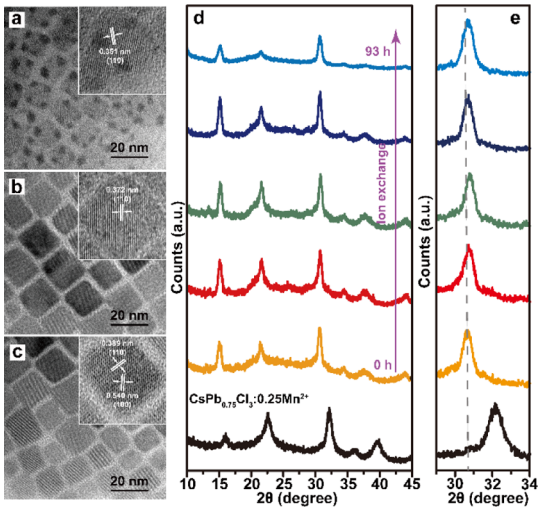

Figure 4. TEM and XRD patterns of the perovskite NCs before and after the ion exchange reaction. (a−c) TEM images of $CsPb_{0.75}Cl_3$:0.25Mn^{2+} NCs, $CsPb_{0.73}Zn_{0.03}Cl_{0.91}Br_{2.05}$:0.22$Mn^{2+}$ NCs (0.05 h), and $CsPb_{0.71}Zn_{0.20}Cl_{0.95}Br_{2.01}$:0.06$Mn^{2+}$ NCs (45 h). Scale bar is 20 nm. (d,e) XRD patterns of pristine $CsPb_{0.75}Cl_3$:0.25Mn^{2+} NCs and ion exchanged NCs obtained at different reaction times.

DOI: 10.1021/acsami.7b18750
ACS Appl. Mater. Interfaces 2018, 10, 11739−11746

JCPDS 18-0366). The ion exchange reactions preserved the crystal phase of the NCs (Figure 4d). The XRD patterns of ion exchanged NCs could be ascribed to the same cubic phase. As expected, upon ion exchange, the cell expanded and the peaks shifted to lower angles for the sample obtained after 0.05 h, whereas the incorporation of Zn^{2+} resulted in some shrinking of the cell and the peaks shifted to higher angles for the samples obtained with a longer reaction time (Figure 4e).

The energy level diagram of Mn^{2+}-doped $CsPb(Cl_yBr_{1-y})_3$ QDs is schemed in Figure 5. As is shown, the $CsPb(Cl_yBr_{1-y})_3$

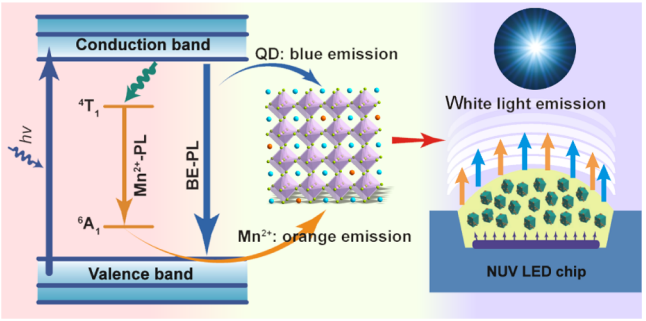

Figure 5. Schematic energy level diagram of Mn^{2+}-doped $CsPb(Cl_yBr_{1-y})_3$ QDs suggesting the unification of tunable BE emission and Mn^{2+} doping luminescence from the perovskites QDs and the designed strategy of white light emission originated from the blue and orange light is also demonstrated.

host absorbs the energy and emits a BE emission via BE electron–hole recombination. As discussed above, the band gap of perovskite QDs is controlled by the ratio of halogen, which results in the tunable of BE emission wavelength. Simultaneously, the doping of Mn^{2+} generates the new recombination pathway of the Mn^{2+}-based d–d transition ($^4T_1$–$^6A_1$) based on the exciton-to-Mn^{2+} energy transfer and finally emits the orange emission, as marked by the corresponding emission lines in Figure 5. Therefore, the white light emission perovskite QDs could be obtained by the combination of the blue emission of BE PL and the orange emission from Mn^{2+} PL. Then, a white light LED could be achieved by using the white light emission perovskite QDs as the color conversion materials, as given in the model in Figure 5. That is to say, in the doped perovskite NCs, an expected halide ratio in the product NCs and the Mn^{2+} doping content could be obtained by controlling the amount of the used halide precursor, allowing one to finely tune the emission wavelength, even the white emission.[35,36]

To start with, the $ZnBr_2$ acts as the bromide precursor to react with the pristine $CsPb_{0.82}Cl_3$:0.18Mn^{2+} NCs to produce a series of Mn^{2+}-doped perovskite NCs with different Cl^-/Br^- ratios in this system. The optical absorption and PL emission spectra of the pristine and these series products are shown in Figure 6a,b. The absorption edge shifts from the about 400 to 460 nm depending on the increasing $ZnBr_2$ contents from 25 to 1250 μL. PL spectra contain a narrow BE emission that is tunable across a wide range depending on different $ZnBr_2$ contents and the fixed Mn^{2+} emission peak. With the increasing amount of the bromide precursor, the BE PL peak shifts monotonically to the red, whereas the Mn^{2+} emission stays nearly constant in energy throughout the exchange process. The relative intensity of Mn^{2+} and BE emission decreased with the increasing bromide content, which is consistent with the discussion above. Therefore, white light can be obtained from the selected sample of $CsPb_{0.76}Zn_{0.014}Cl_{0.93}Br_{2.06}$:0.08$Mn^{2+}$ (with emission peak at 474 nm originated from BE emission and orange light emission peaked at 598 nm from the Mn^{2+} dopant), as also demonstrated in the previous model in Figure 5. Thus, a prototype white light LED device has been fabricated

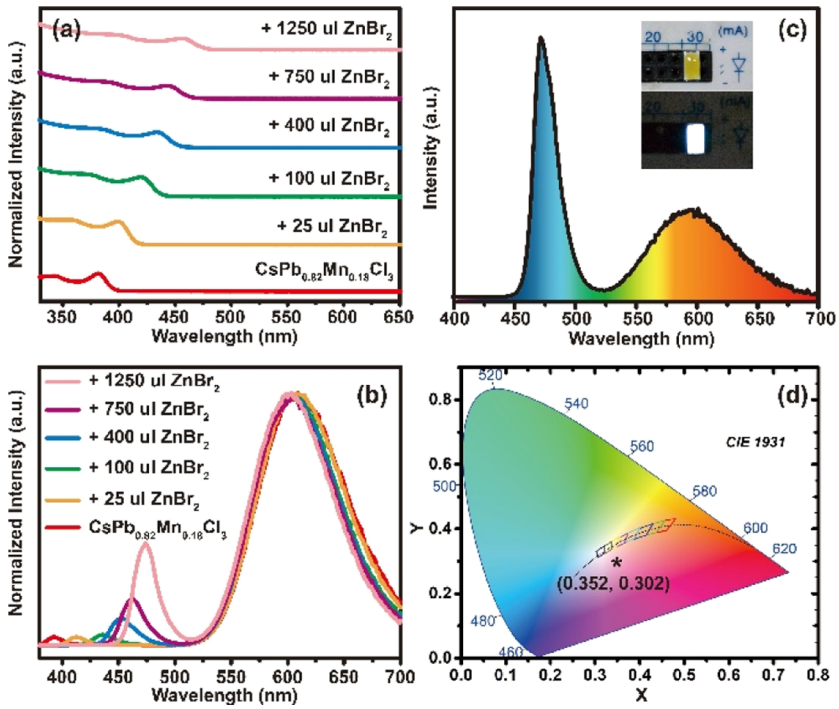

Figure 6. Optical absorption (a) and PL (b) spectra of NCs with different halide ratios. (c) PL spectrum of the LED fabricated from $CsPb_{0.76}Zn_{0.014}Cl_{0.93}Br_{2.06}$:0.08$Mn^{2+}$ NCs and the 365 nm UV LED chip, inset: photograph of the corresponding LED device, and (d) CIE chromaticity coordinates of white LED.

DOI: 10.1021/acsami.7b18750
ACS Appl. Mater. Interfaces 2018, 10, 11739–11746

by using a 365 nm UV LED chip and the $CsPb_{0.76}Zn_{0.014}Cl_{0.93}Br_{2.06}$:0.08$Mn^{2+}$ NCs. The LED device exhibits bright white light emission with the color coordinate of (0.352, 0.302), as shown in Figure 6c, and a photograph of the corresponding device is shown in the inset. The color render index values of the fabricated white LEDs are not high (42 for the $CsPb_{0.76}Zn_{0.014}Cl_{0.93}Br_{2.06}$:0.08$Mn^{2+}$ NCs) because of the strong blue emission. Figure 6d demonstrated the CIE chromaticity coordinate of the as-fabricated white LEDs lamp, suggesting the realization of the high quality white light by such a way.

CONCLUSION

In summary, strong Mn^{2+} emission in high Br^- content $Cs(Pb_{1-x-z}Zn_z)(Cl_yBr_{1-y})_3$:x$Mn^{2+}$ perovskite NCs was first realized through the ion exchange reaction occurring between $ZnBr_2$ and preformed $CsPb_{1-x}Cl_3$:xMn^{2+} NCs, where the rate of anion exchange is much faster than that of cation exchange. The Mn^{2+} substitution ratio reached 22% in the exchanged product of $Cs(Pb_{1-x-z}Zn_z)(Cl_yBr_{1-y})_3$:x$Mn^{2+}$ NCs, which could not be obtained by the direct synthesis method or halogen exchange method used in previous work. By controlling the ion exchange reaction time, the intensity of Mn^{2+} emission can be varied at all through the replacement of Mn^{2+} by Zn^{2+} and thereby the intensity ratio between Mn^{2+} emission and BE emission. As a result, white light-emitting perovskite NCs could be obtained by this RIEE mechanism and be used as new color conversion materials in a prototype LED device based on the commercially available 365 nm LED chip.

ASSOCIATED CONTENT

Supporting Information

The Supporting Information is available free of charge on the ACS Publications website at DOI: 10.1021/acsami.7b18750.

HRTEM image and TEM image of pristine $CsPb_{0.92}Cl_3$:0.08Mn^{2+} (PDF)

AUTHOR INFORMATION

Corresponding Author

*E-mail: xiazg@ustb.edu.cn.

ORCID

Zhiguo Xia: 0000-0002-9670-3223
Caofeng Pan: 0000-0001-6327-9692
Yue Gong: 0000-0002-5764-3117
Lin Gu: 0000-0002-7504-031X
Quanlin Liu: 0000-0003-3533-7140
Jin Z. Zhang: 0000-0003-3437-912X

Notes

The authors declare no competing financial interest.

ACKNOWLEDGMENTS

The authors thank the support from National Natural Science Foundation of China (nos. 51722202, 91622125, and 51572023) and Natural Science Foundations of Beijing (2172036).

REFERENCES

(1) Song, J.; Li, J.; Li, X.; Xu, L.; Dong, Y.; Zeng, H. Quantum Dot Light-Emitting Diodes Based on Inorganic Perovskite Cesium Lead Halides ($CsPbX_3$). *Adv. Mater.* **2015**, *27*, 7162−7167.

(2) Wang, Y.; Li, X.; Nalla, V.; Zeng, H.; Sun, H. Solution-Processed Low Threshold Vertical Cavity Surface Emitting Lasers from All-Inorganic Perovskite Nanocrystals. *Adv. Funct. Mater.* **2017**, *27*, 1605088.

(3) Lu, J.; Sheng, X.; Tong, G.; Yu, Z.; Sun, X.; Yu, L.; Xu, X.; Wang, J.; Xu, J.; Shi, Y.; Chen, K. Ultrafast Solar-Blind Ultraviolet Detection by Inorganic Perovskite $CsPbX_3$ Quantum Dots Radial Junction Architecture. *Adv. Mater.* **2017**, *29*, 1700400.

(4) van der Stam, W.; Geuchies, J. J.; Altantzis, T.; van den Bos, K. H. W.; Meeldijk, J. D.; Van Aert, S.; Bals, S.; Vanmaekelbergh, D.; de Mello Donega, C. Highly Emissive Divalent Ion Doped Colloidal $CsPb_{1-x}M_xBr_3$ Perovskite Nanocrystals through Cation Exchange. *J. Am. Chem. Soc.* **2017**, *139*, 4087−4097.

(5) Wang, L.; Williams, N. E.; Malachosky, E. W.; Otto, J. P.; Hayes, D.; Wood, R. E.; Guyot-Sionnest, P.; Engel, G. S. Scalable Ligand-Mediated Transport Synthesis of Organic-Inorganic Hybrid Perovskite Nanocrystals with Resolved Electronic Structure and Ultrafast Dynamics. *ACS Nano* **2017**, *11*, 2689−2696.

(6) Zhang, F.; Zhong, H.; Chen, C.; Wu, X.-g.; Hu, X.; Huang, H.; Han, J.; Zou, B.; Dong, Y. Brightly Luminescent and Color-Tunable Colloidal $CH_3NH_3PbX_3$ (X = Br, I, Cl) Quantum Dots: Potential Alternatives for Display Technology. *ACS Nano* **2015**, *9*, 4533−4542.

(7) Yakunin, S.; Protesescu, L.; Krieg, F.; Bodnarchuk, M. I.; Nedelcu, G.; Humer, M.; De Luca, G.; Fiebig, M.; Heiss, W.; Kovalenko, M. V. Low-Threshold Amplified Spontaneous Emission and Lasing from Colloidal Nanocrystals of Caesium Lead Halide Perovskites. *Nat. Commun.* **2015**, *6*, 8515.

(8) Su, R.; Diederichs, C.; Wang, J.; Liew, T. C. H.; Zhao, J.; Liu, S.; Xu, W.; Chen, Z.; Xiong, Q. Room-Temperature Polariton Lasing in All-Inorganic Perovskite Nanoplatelets. *Nano Lett.* **2017**, *17*, 3982−3988.

(9) Zhang, X.; Lin, H.; Huang, H.; Reckmeier, C.; Zhang, Y.; Choy, W. C. H.; Rogach, A. L. Enhancing the Brightness of Cesium Lead Halide Perovskite Nanocrystal Based Green Light-Emitting Devices through the Interface Engineering with Perfluorinated Ionomer. *Nano Lett.* **2016**, *16*, 1415−1420.

(10) Vashishtha, P.; Halpert, J. E. Field-Driven Ion Migration and Color Instability in Red-Emitting Mixed Halide Perovskite Nanocrystal Light-Emitting Diodes. *Chem. Mater.* **2017**, *29*, 5965−5973.

(11) Lou, S.; Xuan, T.; Yu, C.; Cao, M.; Xia, C.; Wang, J.; Li, H. Nanocomposites of $CsPbBr_3$ Perovskite Nanocrystals in An Ammonium Bromide Framework with Enhanced Stability. *J. Mater. Chem. C* **2017**, *5*, 7431−7435.

(12) Xuan, T.; Yang, X.; Lou, S.; Huang, J.; Liu, Y.; Yu, J.; Li, H.; Wong, K.-L.; Wang, C.; Wang, J. Highly Stable $CsPbBr_3$ Quantum Dots Coated with Alkyl Phosphate for White Light-Emitting Diodes. *Nanoscale* **2017**, *9*, 15286−15290.

(13) Parobek, D.; Roman, B. J.; Dong, Y.; Jin, H.; Lee, E.; Sheldon, M.; Son, D. H. Exciton-to-Dopant Energy Transfer in Mn-Doped Cesium Lead Halide Perovskite Nanocrystals. *Nano Lett.* **2016**, *16*, 7376−7380.

(14) Jahandar, M.; Heo, J. H.; Song, C. E.; Kong, K.-J.; Shin, W. S.; Lee, J.-C.; Im, S. H.; Moon, S.-J. Highly Efficient Metal Halide Substituted $CH_3NH_3I(PbI_2)_{1-x}(CuBr_2)_x$ Planar Perovskite Solar Cells. *Nano Energy* **2016**, *27*, 330−339.

(15) Abdi-Jalebi, M.; Dar, M. I.; Sadhanala, A.; Senanayak, S. P.; Franckevičius, M.; Arora, N.; Hu, Y.; Nazeeruddin, M. K.; Zakeeruddin, S. M.; Grätzel, M.; Friend, R. H. Impact of Monovalent Cation Halide Additives on the Structural and Optoelectronic Properties of $CH_3NH_3PbI_3$ Perovskite. *Adv. Energy Mater.* **2016**, *6*, 1502472.

(16) Mir, W. J.; Jagadeeswararao, M.; Das, S.; Nag, A. Colloidal Mn-Doped Cesium Lead Halide Perovskite Nanoplatelets. *ACS Energy Lett.* **2017**, *2*, 537−543.

(17) Adhikari, S. D.; Dutta, S. K.; Dutta, A.; Guria, A. K.; Pradhan, N. Chemically Tailoring the Dopant Emission in Manganese-Doped $CsPbCl_3$ Perovskite Nanocrystals. *Angew. Chem., Int. Ed.* **2017**, *56*, 8746−8750.

DOI: 10.1021/acsami.7b18750
ACS Appl. Mater. Interfaces 2018, 10, 11739−11746

(18) Huang, G.; Wang, C.; Xu, S.; Zong, S.; Lu, J.; Wang, Z.; Lu, C.; Cui, Y. Postsynthetic Doping of $MnCl_2$ Molecules into Preformed $CsPbBr_3$ Perovskite Nanocrystals via A Halide Exchange-Driven Cation Exchange. *Adv. Mater.* **2017**, *29*, 1700095.
(19) Liu, H.; Wu, Z.; Shao, J.; Yao, D.; Gao, H.; Liu, Y.; Yu, W.; Zhang, H.; Yang, B. $CsPb_xMn_{1-x}Cl_3$ Perovskite Quantum Dots with High Mn Substitution Ratio. *ACS Nano* **2017**, *11*, 2239−2247.
(20) Zou, S.; Liu, Y.; Li, J.; Liu, C.; Feng, R.; Jiang, F.; Li, Y.; Song, J.; Zeng, H.; Hong, M.; Chen, X. Stabilizing Cesium Lead Halide Perovskite Lattice through Mn(II) Substitution for Air-Stable Light-Emitting Diodes. *J. Am. Chem. Soc.* **2017**, *139*, 11443−11450.
(21) Liu, W.; Lin, Q.; Li, H.; Wu, K.; Robel, I.; Pietryga, J. M.; Klimov, V. I. Mn^{2+}-Doped Lead Halide Perovskite Nanocrystals with Dual-Color Emission Controlled by Halide Content. *J. Am. Chem. Soc.* **2016**, *138*, 14954−14961.
(22) Rossi, D.; Parobek, D.; Dong, Y.; Son, D. H. Dynamics of Exciton-to-Mn Energy Transfer in Mn-Doped $CsPbCl_3$ Perovskite Nanocrystals. *J. Phys. Chem. C* **2017**, *121*, 17143−17149.
(23) Li, F.; Xia, Z.; Gong, Y.; Gu, L.; Liu, Q. Optical Properties of Mn^{2+} Doped Cesium Lead Halide Perovskite Nanocrystals via A Cation-Anion Co-substitution Exchange Reaction. *J. Mater. Chem. C* **2017**, *5*, 9281−9287.
(24) Akkerman, Q. A.; D'Innocenzo, V.; Accornero, S.; Scarpellini, A.; Petrozza, A.; Prato, M.; Manna, L. Tuning the Optical Properties of Cesium Lead Halide Perovskite Nanocrystals by Anion Exchange Reactions. *J. Am. Chem. Soc.* **2015**, *137*, 10276−10281.
(25) Guhrenz, C.; Benad, A.; Ziegler, C.; Haubold, D.; Gaponik, N.; Eychmüller, A. Solid-State Anion Exchange Reactions for Color Tuning of $CsPbX_3$ Perovskite Nanocrystals. *Chem. Mater.* **2016**, *28*, 9033−9040.
(26) Nedelcu, G.; Protesescu, L.; Yakunin, S.; Bodnarchuk, M. I.; Grotevent, M. J.; Kovalenko, M. V. Fast Anion-Exchange in Highly Luminescent Nanocrystals of Cesium Lead Halide Perovskites ($CsPbX_3$, X = Cl, Br, I). *Nano Lett.* **2015**, *15*, 5635−5640.
(27) Bol, A. A.; Meijerink, A. Luminescence Quantum Efficiency of Nanocrystalline ZnS: Mn^{2+}. 1. Surface Passivation and Mn^{2+} Concentration. *J. Phys. Chem. B* **2001**, *105*, 10197−10202.
(28) Beaulac, R.; Archer, P. I.; van Rijssel, J.; Meijerink, A.; Gamelin, D. R. Exciton Storage by Mn^{2+} in Colloidal Mn^{2+}-Doped CdSe Quantum Dots. *Nano Lett.* **2008**, *8*, 2949−2953.
(29) Dong, Y.; Choi, J.; Jeong, H.-K.; Son, D. H. Hot Electrons Generated from Doped Quantum Dots via Upconversion of Excitons to Hot Charge Carriers for Enhanced Photocatalysis. *J. Am. Chem. Soc.* **2015**, *137*, 5549−5554.
(30) Zeng, R.; Zhang, T.; Dai, G.; Zou, B. Highly Emissive, Color-Tunable, Phosphine-Free Mn:ZnSe/ZnS Core/Shell and Mn:ZnSeS Shell-Alloyed Doped Nanocrystals. *J. Phys. Chem. C* **2011**, *115*, 3005−3010.
(31) Shi, L.; Huang, Y.; Seo, H. J. Emission Red Shift and Unusual Band Narrowing of Mn^{2+} in $NaCaPO_4$ Phosphor. *J. Phys. Chem. A* **2010**, *114*, 6927−6934.
(32) Mahamuni, S.; Lad, A. D.; Patole, S. Photoluminescence Properties of Manganese-Doped Zinc Selenide Quantum Dots. *J. Phys. Chem. C* **2008**, *112*, 2271−2277.
(33) Solé, J.; Bausa, L.; Jaque, D. *An Introduction to the Optical Spectroscopy of Inorganic Solids*; John Wiley & Sons, 2005.
(34) Tong, Y.; Bladt, E.; Aygüler, M. F.; Manzi, A.; Milowska, K. Z.; Hintermayr, V. A.; Docampo, P.; Bals, S.; Urban, A. S.; Polavarapu, L.; Feldmann, J. Highly Luminescent Cesium Lead Halide Perovskite Nanocrystals with Tunable Composition and Thickness by Ultrasonication. *Angew. Chem., Int. Ed.* **2016**, *55*, 13887−13892.
(35) Cottingham, P.; Brutchey, R. L. Compositionally Dependent Phase Identity of Colloidal $CsPbBr_{3-x}I_x$ Quantum Dots. *Chem. Mater.* **2016**, *28*, 7574−7577.
(36) Chung, H.; Jung, S. I.; Kim, H. J.; Cha, W.; Sim, E.; Kim, D.; Koh, W.-K.; Kim, J. Composition-Dependent Hot Carrier Relaxation Dynamics in Cesium Lead Halide ($CsPbX_3$, X = Br and I) Perovskite Nanocrystals. *Angew. Chem., Int. Ed.* **2017**, *56*, 4160−4164.

DOI: 10.1021/acsami.7b18750
ACS Appl. Mater. Interfaces 2018, 10, 11739−11746